Coagulation of Colloids Retained by Porous Wall

P. Harmant and P. Aimar
Laboratoire de Génie Chimique, CNRS, Université Paul Sabatier, 31062 Toulouse, Cedex, France

The structure of a colloidal deposit retained by a porous wall is described, accounting for surface interactions and hydrodynamic forces. The balance of forces acting over spherical, charged particles allows the calculation of the interparticular distances inside the cake according to the physicochemical conditions (ionic strength, particle potential, pH, particle size) and to the experimental parameters (flux). The model predicts that beyond a critical mass deposited on the porous wall, the structure of the layers near the membrane changes where the particles are in close contact with each other. Experimental data obtained with latex monodisperse particles filtered over various types of ultrafiltration membranes for various physicochemical and flux conditions are compared to the model predictions. These results explain the existence of irreversible colloidal deposits in filtration and suggest strategies to optimize backflush or pulsed pressure procedures often used to improve the efficiency of ultrafiltration or microfiltration.

Introduction

Membrane processes are used to fractionate fluids such as milk, fermentation broths, and paints from the chemical or biotechnological industries. Since colloids and macromolecular solutes are often simultaneously present, membranes often aim at achieving total rejection for large components and complete transmission for small solutes (such as clarification or protein purification). Under permeate convection, larger particles accumulate on the membrane forming a deposit, and tangential circulation of the fluid on the high-pressure side of the membrane is now the classic way of reducing the growth of such accumulations. However, for some applications engineers wonder if cross-flow filtration presents real advantages (solute denaturation, energy costs) compared to dead-end filtration combined with periodic back-flushing. Such backflushing is efficient provided a certain degree of deposit reversibility is maintained. The whole process has a chance of being economically worthwhile if the cake formation time is easy to determine and long enough (*Low Pressure Membrane Filtration for Particle Removal,* 1992). Optimizing filtration parameters often requires extensive preliminary experiments on a pilot scale.

Whenever the cake takes over from the membrane itself in terms of flux and selectivity, fluid fractionation requires two different levels of understanding of cake formation: deposition kinetics and structure of the deposit as a function of hydrodynamic and physicochemical conditions.

Correspondence concerning this article should be addressed to P. Aimar.

Colloidal fouling of membranes poses specific problems for engineers. Green and Belfort (1980) have shown that the simple film model underestimates permeate limiting fluxes in the case of suspensions. According to particle sizes, several phenomena have been invoked to explain this "colloidal flux anomaly," for large particles (over 1 μm), hydrodynamic contributions, such as shear induced diffusion (Zydney and Colton, 1986) or tubular pinch effect (Green and Belfort, 1980) are invoked. Concerning medium-size particles (0.1 – 1 μm), Bacchin et al. (1995) have studied the influence of surface forces.

Such forces play a major role not only in the stability of colloidal suspensions (Verwey and Overbeek, 1948) but also in particle adhesion on surfaces (Elimelech, 1994) and in membrane fouling (Cohen and Probstein, 1986; McDonogh et al., 1989) due to the high surface to volume ratio of colloidal particles. Bacchin et al. (1995) link the deposition rate to the hydrodynamic conditions and physicochemical properties of the suspension (diffusion and surface interactions). Assuming that particles are independent from each other in the bulk and using a perfect sink boundary condition at the fluid-cake interface, they derive an expression for the critical flux. When the operating flux is larger than this critical value, colloids deposit at the membrane surface according to a standard filtration law. If the flux is lower than this threshold, there should not be any deposit. Experiments with a suspension of clay are in good agreement with the model's predictions. As Bacchin et al. (1995) use a perfect sink boundary,

their model cannot provide any information on the particle behavior in the deposit. However, this behavior can have a tremendous effect on cake reversibility and hydraulic resistivity.

The buildup of colloidal filter cakes has received less attention. Most studies consider the filter cake as an isotropic phase and study global effects of the suspension physico-chemistry on its specific resistivity. Statistical models, based on particle adhesion (or capture efficiency) as a function of incidence and velocity suggest the existence of dendritic layers (Schmitz et al., 1993) or of global cake resistance variations (Sherman and Sherwood, 1993).

Purely mechanical analyses have been proposed (Leonard and Vassilieff, 1984; Romero and Davis, 1988) and put forward classic mass balance, incorporating viscosity variations in the boundary layer due to an increase in particle concentration. Romero and Davis show that under some conditions, a stagnant layer of packed particles exists beneath a flowing layer at a lower concentration than the packed one.

The first models, developed for the case of the filter-press (Tiller and Crump, 1977), based on a force balance incorporating particle-particle interactions have been transposed to membrane separations (McDonogh et al., 1989, 1992). The main results concern the packing gradient, which increases across the cake layer from the bulk side towards the membrane side. Very similar results were developed with regard to ceramic processing applications, especially slip casting (Tiller and Tsai, 1986; Hampton et al., 1988). Specific cake resistance is also often related to pH, ionic strength, and particle size. A similar model has recently been developed by Bowen and Jener (1993).

These approaches often involve empirical coefficients and describe the cake as a static medium. The cake is assumed to be an infinite phase, and a global balance of forces cannot be solved entirely because of the absence of limiting conditions. This requires empirical coefficients to fit experimental results. Thus, these studies do not provide accurate information on the characteristics of the cake during filtration. Moreover, these models do not take into account both permeate flux and deposited mass as parameters.

Recent operating procedures involving "pulsed" ultrafiltration (Rodgers and Miller, 1993) or a "backshock" process (Wenten, 1995) have been shown to maintain high fluxes and protein transmission despite moderate cross-flow velocities. Previously developed models do not predict such behaviors and so cannot explain them satisfactorily.

The purpose of this article is to discuss the deposit structure (namely interparticular distances) and buildup (reversibility/irreversibility) in the case of colloidal suspensions. This study is based on forces (drag forces and surface interactions) acting over the particles forming the cake. The model does not require introduction of empirical coefficients. With the exception of the Hamaker constant, all the parameters may be easily determined. Results show the existence of two cake structures, according to the surface to drag forces ratio. They describe how particles can aggregate inside the cake during filtration. A critical mass is defined, corresponding to the maximum mass of particles that can be reversibly deposited under given conditions (flux, ionic strength, particle potential). Experimental data obtained with monodisperse latex particles are in good agreement with theoretical predictions. Conclusions are applied to optimizing the control of the ultrafiltration of a colloidal suspension.

Theoretical Development

Interactions between colloidal particles involve forces of different natures (DLVO theory): electrostatic double-layer repulsions, van der Waals attractions, and short-range forces (Born repulsion or hydration forces). At low ionic strength, the total force prevents particles from coagulating (Figure 1). This barrier tends to disappear as ionic strength increases and totally vanishes beyond the critical coagulation concentration (CCC).

Particles about to form a deposit are so close to each other that they can experience mutual interactions, the intensity of which depends predominantly on the distance from the nearest neighbors. In practice, the range of electrostatic repulsions is of about one-hundred nanometers which is quite comparable to particle size. In this article, we shall consider as nearest neighbors the particles belonging to layers immediately above and below the layer studied. Adding interaction force expressions developed for two isolated spheres is valid only when particles are very distant from each other. As the deposit gets more concentrated, this type of calculation becomes approximate. As a one-dimensional flux is assumed, the interactions with neighbors from the same layer just balance each other. Contributions from the second nearest layers are comparatively small as the strength of interaction decreases exponentially with distance at large separation distances. The electrical repulsions experienced by these layers will be screened even more if the relative permeability of the nearest neighbors is taken into account. In fact, the relative permittivity is lower for particles than for water. In the present work, we assume that spherical colloidal particles accumulate in a pattern which can be approximated as a cubic centered lattice (Figure 2).

It can be considered that particles are subject to four effects: diffusion, two surface forces and a viscous force as sketched in Figure 3.

A series of simulations was performed using the following equation proposed by Einstein (Van de Ven, 1989), as diffusional force

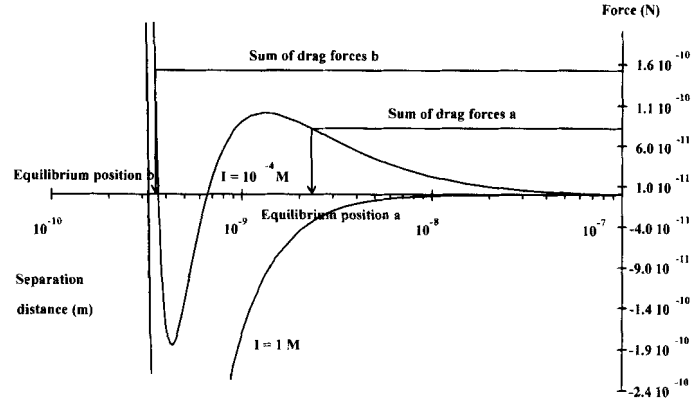

Figure 1. Surface forces vs. shortest separation distance between particles.

Assumption: $a = 220$ nm, Hamaker constant 10^{-20} J, particle potential -65 mV and temperature 20°C.

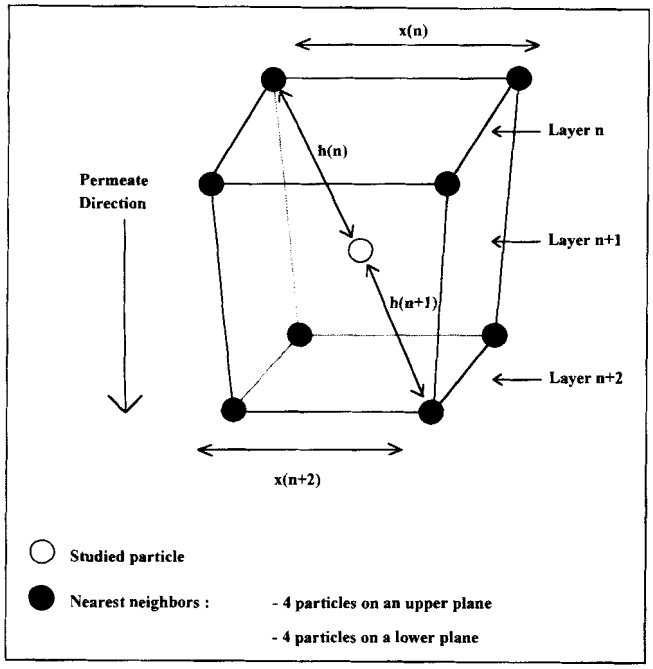

Figure 2. Particular lattice chosen for simulation (cubic centered lattice).

$$F_d = -\frac{kT}{n}\frac{dn}{dx} \quad \text{with } n \text{ the particle concentration } (\text{kg}\cdot\text{m}^{-3}) \tag{1}$$

A simple force balance incorporating Stokes force and F_d would lead to the classic film model. However, F_d is only valid for low concentrated dispersions and this expression must be used only for estimation.

Happel's cell (Happel, 1958) is used to account for the hydrodynamic interactions between particles in the calculation of viscous forces. It introduces a coefficient $f(\gamma)$ to correct the standard Stokes force derived for a single particle in motion in an infinite volume of Newtonian fluid

$$F_v = 6\pi\mu a J \cdot f(\gamma) \tag{2}$$

where $f(\gamma)$ is defined as

$$f(\gamma) = \frac{3+2\gamma^5}{3-9/2\gamma+9/2\gamma^5-3\gamma^6} \tag{3}$$

with

$$\gamma = (1-\epsilon)^{1/3} \tag{4}$$

The local deposit porosity ϵ for a given particle size $f(\gamma)$ is only dependent on the shortest interparticle distance. As shown in Figure 4, a single particle undergoes the standard Stokes force (f(voidage) = 1), whereas in a compact bed (maximum voidage equal to 0.32) the particle is submitted to a force 185 times larger than the Stokes one. Through this approach, the specific resistance $\alpha(\text{s}^{-1})$ is given by

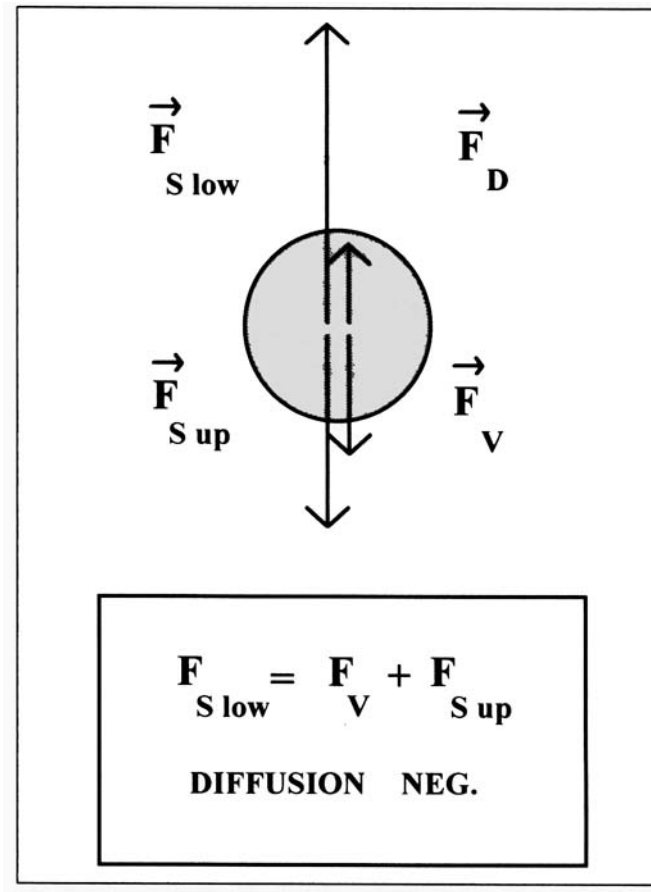

Figure 3. Forces undergone by studied particle.

$$\alpha = 9/2\frac{\mu}{\rho_s a^2}\cdot f(\gamma) \tag{5}$$

More recent results concerning hydrodynamic interactions between the particles have been compared to this theory (Zick and Homsy, 1982). For body-centered cubic arrays, the maximum value of the hydrodynamic factor $f(\gamma)$ is 163. This represents a maximum error of 14%. For the sake of simplicity,

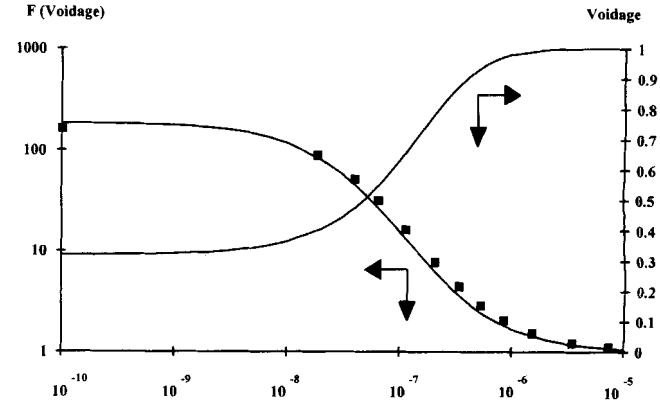

Figure 4. Voidage and coefficient modifying Stokes equation vs. shortest separation distance between particles.

Assumptions: a = 220 nm and temperature 20°C.

we used the classic Happel and Brenner approach, since Zick and Homsy's results are discrete. The symbols in Figure 4 represent these discrete results.

Constant charge double-layer interactions V_w ($kg \cdot m^2 \cdot s^{-2}$) (Wiese and Healy, 1970), unextended unretarded van der Waals interactions V_a (Jia and Williams, 1990), and Born repulsions V_b (Ruckenstein and Prieve, 1973) are used to estimate surface forces.

The choice of constant charge rather than constant potential repulsion is discussed later in the material section. Exact results for the repulsive force, even in the case of two equal spheres, are only available from computation. The solution of the linear Poisson-Boltzmann equation in the case of a constant charge (Wiese and Healy, 1970) describes the exact solution well at intermediate and high separation distances even for highly charged particles at small Ka (Carnie et al., 1994). Unfortunately, this analytical solution is no longer valid at short distances in low molar solutions. Some corrections of this force were made (Glendinning and Russel, 1982) and lead to an acceptable analytical formula for distances greater than the maximum peak force abscissa (Figure 1). Except for that particular case, the Wiese formulation remains the best suited to this type of analysis.

Close repulsive forces were initially included but, as suggested by one of the referees, they were rapidly replaced by a simple nonoverlap condition to speed up calculations.

In the expressions used for this simulation, h is the shortest sphere-to-sphere separation distance (m), as in Figure 2

$$V_w = -\frac{\epsilon_r \epsilon_0 a \psi_0^2}{2} \ln[1 - \exp(-\kappa h)] \quad \text{double-layer repulsions} \quad (6)$$

$$V_a = -\frac{Ha}{12h} \quad \text{van der Waals attraction } (kg \cdot m^2 \cdot s^{-2}) \quad (7)$$

$$V_b = \frac{H\sigma_c^6}{7{,}560}\left(\frac{8a+h}{(2a+h)^7} + \frac{6a-h}{h^7}\right) \quad \text{Born repulsions} \quad (8)$$

with a collision diameter σ_c of 0.5 nm.

The total interactions force F_s (modulus, $kg \cdot m \cdot s^{-2}$) is derived from the total surface potential V_t ($kg \cdot m^2 \cdot s^{-2}$)

$$V_t = V_w + V_a + V_b \quad (9)$$

The force balance (Figure 3) applied to a particle from layer n, projected on the vertical axis (permeate direction), may be written as

$$4/\sqrt{3}\, F_s[h(n)+2a] = 4/\sqrt{3}\, F_s[h(n-1)+2a] + F_v\{[1-\epsilon(n)]^{1/3}\} \quad (10)$$

where $h(n)$ is the shortest separation distance (m) between spheres belonging to levels n and $n+1$

$$\epsilon(n) = 1 - \sqrt{3}\,\pi\left(\frac{a}{[h(n)+h(n-1)]/2+2a}\right)^3 \quad \text{with porosity at level } n \quad (11)$$

except for the first layer (layer in contact with bulk) where equations reduce to

$$4/\sqrt{3}\, F_s[h(1)+2a] = F_v\{[1-\epsilon(1)]^{1/3}\} \quad (12)$$

$$\epsilon(1) = 1 - \sqrt{3}\,\pi\left(\frac{a}{h(1)+2a}\right)^3 \quad \text{with porosity at level 1} \quad (13)$$

The force balance is solved by an iterative routine, layer by layer for each deposited mass. The balance is first solved for the layer in contact with the bulk solution (unknown $h(1)$) and is incremented towards deeper layers (unknown $h(n)$). Equations are solved by a Newton-Raphson method using first derivatives (Press et al., 1986). The hydraulic resistance due to each layer is calculated (specific resistance α (Eq. 5) multiplied by the deposit mass per unit area), the total cake resistance determined and flux decreased assuming permeate flux J ($m \cdot s^{-1}$) is related to trans-membrane pressure ΔP ($kg \cdot m^{-1} \cdot s^{-2}$), to membrane resistance R_m ($kg \cdot m^{-2} \cdot s^{-1}$) and to additional resistance due to fouling R_d (deposit) ($kg \cdot m^{-2} \cdot s^{-1}$)

$$J = \frac{\Delta P}{R_m + R_d} R_d$$

being related to deposited mass m_d(kg): $R_d = \dfrac{\alpha m_d}{S_m}$ (14)

For each increase in mass (deposit of a new layer), the first distance ($h(1)$) was calculated again and the whole routine was repeated.

Two different operating modes were considered, depending on the filtration mode: constant transmembrane pressure or constant permeate flux. Unknowns such as separation distance, specific resistance, deposited mass, and flux (or transmembrane pressure) vs. time were determined. The calculation requires parameters such as ionic strength I ($mol \cdot L^{-1}$), initial permeate flux J, surface potential at set pH and I (ψ_0, assumed to be equal to zeta-potential), particle radius a (m), particle density ρ_s ($kg \cdot m^{-3}$), and Hamaker constant H ($kg \cdot m^2 \cdot s^{-2}$). H was estimated to be 10^{-20} J according to the works of Hull and Kitchener (1969) or Lyklema (1991) for the same type of polymeric colloids.

Results

A first series of simulations, using Eqs. 1, 2, and 9, has shown that in our conditions, and because the Stokes force is increased by the density of particles in layers, diffusion can be neglected in all cases.

In Figure 5, two extreme cases are shown according to the ratio of drag forces to surface forces. At distance 0, the cake is in contact with the membrane whereas at maximum distance, it is in contact with the bulk solution. In the case of a very low ratio of drag to surface forces, the shortest distance between particles gradually decreases as the particles considered are closer to the membrane. These distances are still great (about 60 nm). On the other hand, when the force ratio is large (e.g., same surface forces but higher permeate flux), particles are in close contact with each other (0.3 nm separation) and form a packed layer. This means that particles may

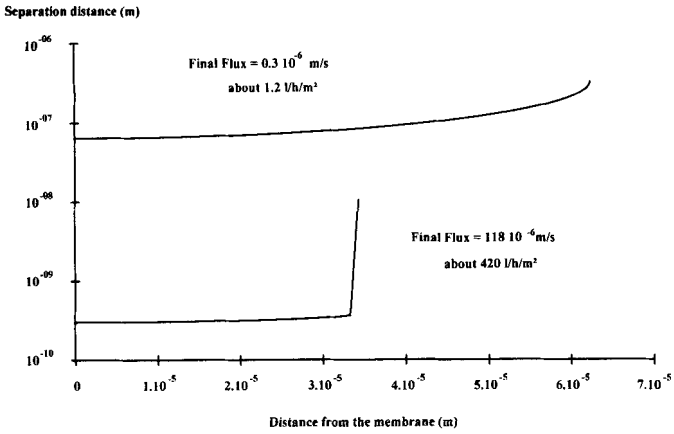

Figure 5. Shortest separation distance between particles vs. distance from the membrane at high and low fluxes.

Assumptions: $a = 220$ nm, Hamaker constant 10^{-20} J, particle potential -65 mV, ionic strength 10^{-4} M, particle density 1,360 kg/m^3 and temperature 20°C.

adsorb onto each other and the cake then acquires a high cohesiveness.

In an intermediate case (Figure 6), corresponding to drag and surface forces of the same order of magnitude, the cake presents two different zones. Close to the membrane, layers are packed, whereas further away they form a loose structure. It should be noted that the order of magnitude of the intermediate flux corresponds to a typical ultrafiltration flux.

The decrease in separation distances as particles are more deeply trapped in the deposit may be explained with the aid of Figure 7.

If $m \rightarrow p$ refers to the force generated by layer m and acting over a particle of layer p, one can write for step $n+1$:

For particles of the first layer

$$F_s(2 \rightarrow 1) = F_v(1) \tag{15}$$

whereas for the second layer

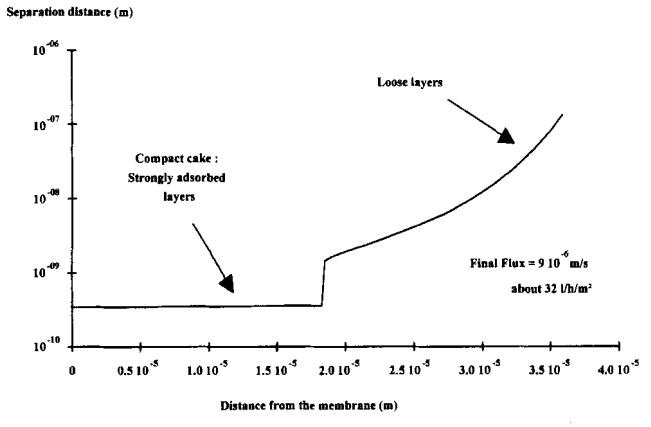

Figure 6. Shortest separation distance between particles vs. distance from the membrane at a medium flux.

Assumptions: $a = 220$ nm, Hamaker constant 10^{-20} J, particle potential -65 mV, ionic strength 10^{-4} M, particle density 1,360 kg/m^3 and temperature 20°C.

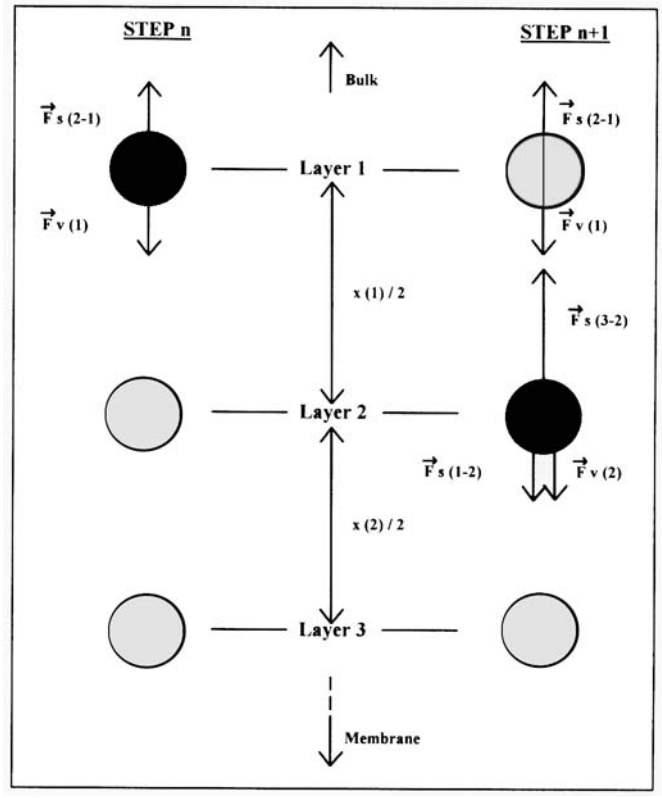

Figure 7. Particles packing and corresponding forces.

$$F_s(3 \rightarrow 2) = F_s(1 \rightarrow 2) + F_v(2) \tag{16}$$

According to the action and reaction principle

$$F_s(2 \rightarrow 1) = F_s(1 \rightarrow 2) \tag{17}$$

which implies that

$$F_s(2 \rightarrow 1) < F_s(3 \rightarrow 2) \tag{18}$$

F_s the total interactions force (modulus, kg·m·s^{-2}) being a decreasing function at a great separation distance, the latter decreases as the considered particle is closer to the membrane.

When particles are in close contact, the particle-particle distance corresponds in Figure 1 to roots of Eqs. 10 or 12 beneath the surface force minimum. Roots corresponding to loose layers are larger than the force-peak maximum abscissa. When the transmembrane pressure is released, particles from compact layers should remain stuck to each other in the vicinity of the membrane due to the existence of a force well, whereas those from loose layers should be free to redisperse in the bulk. This difference creates two zones in a cake, the size of which depends on the solution's properties (pH, ionic strength, and intrinsic particle characteristics) and on the cake buildup conditions (flux, viscosity). One part is reversibly deposited, whereas the other is not. The ability to reexpand when the pressure is released has been studied experimentally. The results of the observations are presented in the next section.

Table 1. Zeta-Potential Values at Different Ionic Strengths

Concn. in NaCl (mol/L)	10^{-4}	3.10^{-4}	10^{-3}	3.10^{-3}	10^{-2}	3.10^{-2}	0.1	0.14	0.28
Corrected Zeta Potential (mV)	−66	−71	−73	−81	−63	−52	−32	−35	−27

Material

A suspension of latex particles was used. The average size was estimated by photon correlation spectroscopy (PCS) and the zeta-potential was measured by microelectrophoresis using a zeta-sister 4 (Malvern) Instrument.

Zeta potential measurements at different ionic strengths and at pH around 6 were quite reproducible. Zeta potential was calculated from mobility using Henry's law. Corrections of the experimental value were made according to O'Brien and White (1978), which take into account ionic strength, electric field alteration, and electrophoretic retardation. Results in Table 1 show a large decrease in zeta potential as electrolyte concentration approaches CCC.

The CCC was estimated to be 0.14 M for sodium chloride. Below this value, particles are independent and do not form aggregates. The average particle size was 220 nm with a standard deviation of 55 nm.

Different calculations of the CCC were made using the van der Waals potential (Eq. 7), Wiese and Healy model (Eq. 6), or constant potential repulsion (Sader et al., 1995). When varying the total salt concentration, the CCC was found when the maximum peak potential equaled kT. Through a constant potential mode, a value of 0.02 M was found whereas constant charge theory leads to 0.08 M. Since the last method gives better agreement with the experimental value, and since the phenomenon described in the cake was close to coagulation, a constant charge approach was preferred in this model. Each filtration experiment was carried out at a salt concentration below this limit, therefore in the absence of aggregates. Particle density was estimated to be 1,360 $kg \cdot m^{-3}$ by measuring the mass of a given volume of known mass concentration.

In the simulations, the particle potential was assumed to be equal to Zeta potential and the average size was considered, thus neglecting the polydispersity.

An ultrafiltration cell (Amicon 8050) with a capacity of 80 mL and effective membrane area $S_m = 1{,}260$ mm^2 was used without stirring in order to control the deposited mass carefully. The Poly Ether Sulfonated (PES) membranes had cutoffs varying from 5 to 100 kDa (Tech-Sep) and their water permeabilities were between $0.2.10^{-9}$ and 10^{-9} $m^2 \cdot s \cdot kg^{-1}$. The selected cutoffs imply no internal fouling or pore blocking. Pressure was adjusted using pressurized air. Before each experiment, membranes were washed for 1 h at 40 kPa with an alkaline cleaning agent (Ultrasil 10, Henkel) at 0.8% by mass, rinsed, and compacted for 1 h under 200 kPa with distilled water. A fresh piece of membrane was used for each experiment. The cell temperature was maintained at 20°C during the experiment. Permeability was then measured at 20°C from the water flux with distilled water. Particle concentration was monitored by turbidty measurement (Hach turbidimeter) after calibration with suspensions of known concentration (a specific calibration curve was made for each ionic strength).

Experimental Procedure

The cell was filled with a 60-g suspension of latex particles with a concentration varying from 0.025% to 0.25% by mass, in accordance with the required deposited mass. About 40 g of suspension was filtered under various conditions of membrane porosity, pressure, and ionic strength, in order to deposit 10 mg to 100 mg. The pressure was then relaxed, the cell cap was removed, and the permeate gently reintroduced into the cell using a syringe. The suspension was then manually stirred at very low speed. This step requires attention in order to avoid tearing of the cake mechanically. The particle concentration of this suspension was then measured at different times and the maximum concentration of resuspended particles was determined. By comparison with the initial concentration, the reversibility fraction was therefore calculated and compared to simulated results.

Experimental Results and Discussion

Results are presented in Figure 8 (deposited mass varying from 10 mg to 100 mg at $I = 10^{-4}$ M) and in Figure 9 (various ionic strengths for a 40 mg deposit). The symbols represent experimental results whereas the lines correspond to the simulation with the corresponding parameters. Trends and quantitative values are in good agreement with the model.

As predicted by the theoretical model, reversibility is total at low final fluxes and gradually decreases as the flux increases. In fact, at low fluxes, the viscous forces are too weak to induce particle coagulation, whereas at high final fluxes, some of the particles from the deepest layers in the filter cake are placed flat on each other.

As the ionic strength increases, the maximum of the repulsive force is reduced and less particles are prevented from coming into contact. As the CCC is approached (here 0.14 M

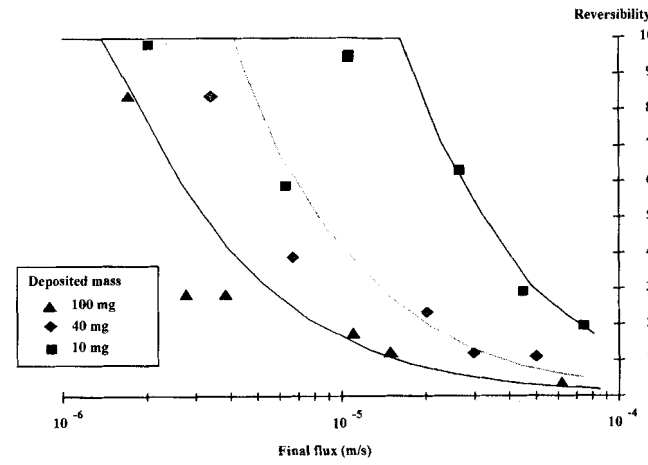

Figure 8. Experimental and theoretical reversibilities vs. final flux for various amounts of deposit.

Symbols represent experimental reversibilities whereas lines correspond to data simulated with: $a = 220$ nm, Hamaker constant 10^{-20} J, particle potential −65 mV, ionic strength 10^{-4} M, particle density 1,360 kg/m^3 and temperature 20°C.

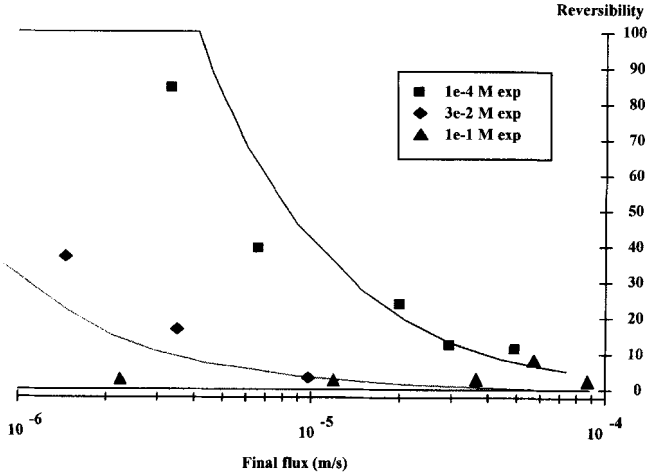

Figure 9. Experimental and theoretical reversibilities vs. final flux for various ionic strengths.

Symbols represent experimental reversibilities whereas lines correspond to data simulated with: $a = 220$ nm, Hamaker constant 10^{-20} J, deposited amount 40 mg, temperature 20°C, particle density 1,360 kg/m^3 and particles potential given in Table 1.

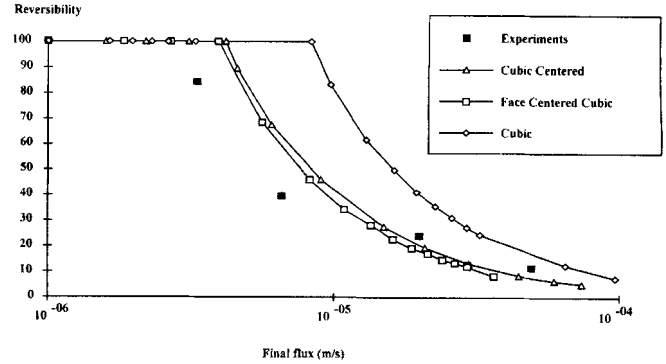

Figure 10. Experimental and theoretical reversibilities vs. final flux for different types of lattices.

Symbols represent experimental reversibilities whereas lines correspond to data simulated with $a = 220$ nm, Hamaker constant 10^{-20} J, deposited amount 40 mg, temperature 20°C, particle density 1,360 kg/m^3, ionic strength 10^{-4} M and particle potential -65 mV.

in NaCl), the repulsive force totally vanishes and reversibility is poor whatever the final flux (drag forces are not balanced).

For a given final flux, reversibility decreases when the deposited mass is increased. As more layers are added at the top of the cake, the reference particle undergoes an ever stronger global viscous force. So long as the sum of the drag forces is balanced by surface repulsions between this reference particle and the layer underneath (case a in Figure 1), a certain distance is maintained between particles. When this sum of drag forces overcomes the double-layer repulsions (total viscous force crosses over the maximum peak of the surface force), the reference particle comes into close contact with the particles on the layer just below it (case b in Figure 1). This phenomenon is a coagulation promoted by the drag forces through the loose cake. This model therefore completes previous approaches. In particular, it shows that even if a flux is not strong enough to bring a single particle into close contact with a membrane surface (flux < critical flux), there may be deposition conditions for which hydrodynamic interactions between particles of a loose layer drive to the deposition of particles in close contact.

In practice, when a filtration experiment is carried out at low ionic strength, the first particles are expected to deposit in a loose form. If the deposited amount reaches a critical value, which depends on the physicochemical properties of the particle, pH, ionic strength and permeate flux, any additional layer causes irreversible coagulation of the layer at the interface between the loose and the packed fraction of the cake. So, particles arriving at the top of the filter cake cause a dense zone to appear near the membrane. The overall mass of particles deposited in a loose form then remains constant while the mass of packed layers increases beyond the critical mass (a moving boundary appears between the loose and the packed layers). Irreversibility therefore increases with the deposited mass because the percentage of particles deposited in a compact ordering is increased.

Different lattices (i.e., a face centered cubic lattice or simple cubic lattice) were considered in the simulation. Computation shows in Figure 10 that the type of lattice has little influence on the average separation distances and on cake permeability. Finally, the CC lattice was preferred because of its higher probability as particles arriving over the cake are likely to deposit in a zone of higher flux (i.e., at the center of a square structure). In other words, the streamlines pass between already deposited particles.

The way this coagulation occurs can be compared to the mechanism assumed in the gel polarization model in ultrafiltration of macromolecules (Michaels, 1968). In the latter, when the *Pe* number in the boundary layer goes beyond a critical value, the concentration profile in the boundary layer is such that the wall concentration exceeds the solubility limit, whereas in this model hydrodynamic forces overcome the colloid stability limit.

A decrease in the range of particle repulsions (by increasing ionic strength) or in their strength (by decreasing particle potential (namely with pH)), or an increase in drag forces (higher fluxes), minimizes the value of the critical mass or, in other words, increases irreversibility for a given deposited mass.

Control of a Separation Operation

The above conclusions were applied to control the ultrafiltration of a latex suspension at a set filtration rate, with the objective of minimizing the increase in transmembrane pressure due to fouling. Cycles were conducted in dead-end mode and repeated for 90 min. Different cycle durations allowed different amounts per cycle to be deposited on the membrane. At the end of each cycle, the stirrer was switched on and the pressure was released to allow resuspension of particles deposited in loose layers. After 2 min, stirring was stopped and a new cycle began. Stirring speed was adjusted to enhance diffusional migration of loose layers back into the bulk solution and to avoid shear induced erosion.

An experiment without stirring for 90 min was carried out and used as a reference of total nonreversibility. The additional hydraulic resistance vs. time ratio was calculated from the pressure increase according to the standard theory of additive resistances.

Experimental Procedure and Results

The cell was filled with the suspension of calibrated latex particles at a concentration of 1.6% by mass except for the experiment at the lowest deposited mass per cycle m_d (kg), where it was 0.4% by mass. Diafiltration experiments were conducted at a set permeate flow rate of 0.5 mL/min supplied by an LKB Bromma 2150 HPLC pump on PES 40 kDa membranes. Before each run, membrane permeability was determined from water flux measurements at 20°C with distilled water. The diafiltration solvent had an ionic strength of $I = 10^{-4}$ mol/L. Cycles varied in length from 2 to 12 min. Shorter sequences were not possible because of the slow pressure actuation, and this led us to use a more dilute suspension to attain lower values of m_d. A pressure gauge monitored the transmembrane pressure during the experiments.

Figure 11 shows the additional cake resistances, determined from pressure readings, assuming traditional additive resistances (Eq. 14).

As expected, the 90 min cycle shows proportionality between additional resistance and time and gives the maximum fouling reference for this set of experiments. As the mass deposited per cycle decreases, the irreversible fraction of colloidal fouling is reduced; below a critical mass (between 8 and 13.5 g/m^2/cycle), the system presents an absence of significant irreversible deposit. More precisely, at the end of a cycle, stirring removes residual fouling from the membrane in the case of loose deposition.

A global reversibility may be calculated from the plot of R_d at the end of cycle vs. time, since global reversibility (% Rev) is given by

$$\%\text{Rev} = 100\left(1 - \left(\frac{\Delta R_d}{\Delta t}\right)\frac{1}{\alpha_m J c_b}\right) \tag{19}$$

where α_m represents the specific resistance of packed layers (s^{-1}) (i.e., maximum specific resistance whatever the physicochemical and operating parameters may be). This value was compared to simulated results and to experimental values given in the previous section in Figure 12.

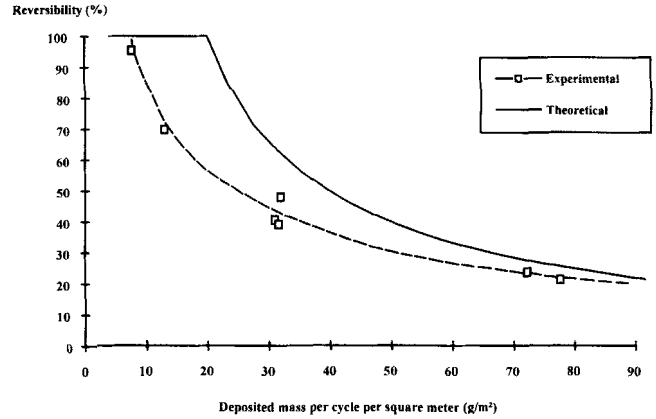

Figure 12. Global reversibility vs. deposited mass per cycle and per unit area.

Results are obtained from the slopes of experimental results presented in Figure 11 according to Eq. 19. Simulations with data: $a = 220$ nm, Hamaker constant 10^{-20} J, particle potential -65 mV, ionic strength 10^{-4} M, particle density 1,360 kg/m^3, constant flux $6.63.10^{-6}$ m/s and temperature 20°C.

The curves are similar except for a small drift in magnitude. This shift could be attributed to the experimental procedure, in which the time between cycles was quite short (2 min): in fact, in zones where the shear stress is poor due to the magnetic stirrer geometry (disk in the center or near cell walls), particles did not have enough time to diffuse back to the bulk solution.

Considering the particles used in this work, a critical mass may be defined as a function of ionic strength, particle potential and permeate flux. In Figure 13, computed critical mass is plotted vs. the ionic strength for various particle potentials for a given constant flux (10^{-5} m/s). The critical mass was found to be proportional to the reciprocal of permeate flux. For example, for permeate fluxes J_1 and J_2 and same physicochemical conditions, the corresponding critical masses m_{cr1} and m_{cr2} are linked by

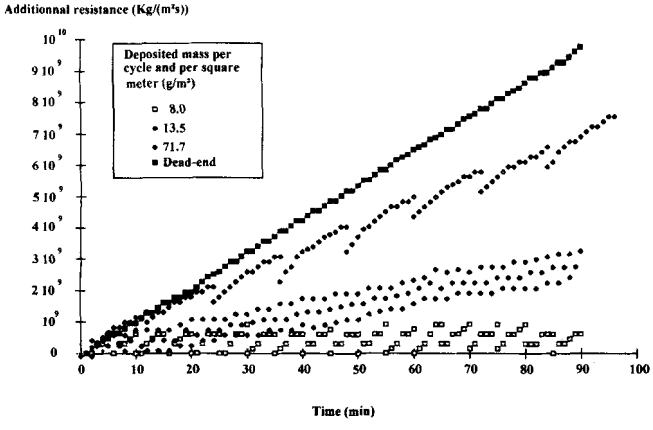

Figure 11. Experimental additional resistance R_d vs. time for various deposited amounts per cycle.

Experiments were conducted at 10^{-4} M ionic strength and temperature 20°C. $R_m = 0.59 \times 10^9$ kg/(m^2·s).

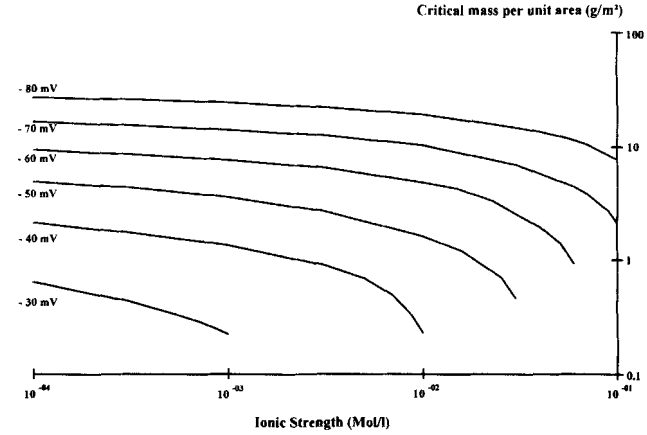

Figure 13. Simulated critical mass per unit area vs. ionic strength for various particle potentials.

Lines correspond to simulations with data: $a = 220$ nm, Hamaker constant 10^{-20} J, constant flux 10^{-5} m/s, temperature 20°C and particle density 1,360 kg/m^3.

$$m_{cr1} = m_{cr2}\frac{J_2}{J_1} \tag{20}$$

The curves in Fig. 13 can be used to estimate theoretical critical masses at any flux. This simulation may allow a theoretical estimation of the critical mass value for other colloidal systems.

Conclusion

The buildup of particle cakes on an unstirred porous wall is influenced by a balance between drag and surface forces. If the drag force on a particle is stronger than the repulsion, a physical adsorption (primary energy minimum) can occur. Otherwise, the distance between particles for which the drag force balances the surface repulsion is quite large, and the cake thus formed has a loose, perfectly reversible structure.

In the case of a multilayer loose cake, a force balance shows that the total drag force experienced by the first layer of this loose cake increases with the number of layers of cake. The calculations show that if the number of layers exceeds a threshold value, then the drag force exerted on the first layer is greater than the maximum electrostatic repulsion between the first layer of the loose cake and the last one of the compact cake underneath.

As a consequence, the first layer of the loose cake collapses and aggregates onto the packed cake, therefore forming a moving boundary between packed and loose parts.

The number of layers reversibly deposited first increases to a threshold, then remains constant; thus, the number of irreversibly packed layers is nil at the beginning and increases only when the critical mass has been reached. The irreversibility percentage of the deposit therefore follows the same trend. The value of the critical mass depends on particle potential, particle size, particle density, flux and ionic strength: quantitative data for spherical particles can be estimated from Figure 13. Phenomena, similar to those described in this article, could well occur in the transport of fines in soils or even in centrifugation.

This result is of great importance in the control of pressure driven membrane processes. It is desirable so as to control experimental parameters that the critical mass should not be exceeded in order to avoid irreversible colloidal fouling. The control of the loose/packed layer ratio, which governs the full reversibility of the separation, is made possible by pulsed flow, as demonstrated in this article. The separation may be preceded by adjustments of ionic strength or pH (to increase particle potential) to increase the critical mass at a required flux. Moreover, in the case of fluid fractionation, reaching the critical mass may induce a considerable reduction in equivalent pore size and could trap solutes at the moving boundary between loose and packed layers. Such conclusions could be useful in fields where the transmission of small solutes across particular cakes is studied (such as fractionation and transport in soils).

Acknowledgment

This work was supported by an EEC AAIR contract no. CEC-AIR2 CT93.1207.

Notation

a = particle radius, m
C_b = bulk concentration, $kg \cdot m^{-3}$
F_d = fictitious diffusional force (modulus), $kg \cdot m \cdot s^{-2}$
F_s = total surface interactions force (modulus), $kg \cdot m \cdot s^{-2}$
F_v = viscous force (modulus), $kg \cdot m \cdot s^{-2}$
k = Boltzmann constant, $kg \cdot m^2 \cdot s^{-2} \cdot K^{-1}$
m_{cr} = critical mass per square meter, $kg \cdot m^{-2}$
ΔP = transmembrane pressure, $kg \cdot m^{-1} \cdot s^{-2}$
t = time, s
T = temperature, °C
V_b = steric potential, $kg \cdot m^2 \cdot s^{-2}$
$X(n)$ = lattice dimension on layer n, m
ϵ_r = relative dielectric constant, $\epsilon_r = 78$
ϵ_0 = absolute dielectric constant, $\epsilon_0 = 8.85 \times 10^{-12}$ $F \cdot m^{-1}$
γ = sphere radius ratio (Happel's model)
κ = reciprocal Debye length, m^{-1}
μ = solvent viscosity, $kg \cdot m^{-1} s \cdot^{-1}$
ρ_s = powder density, $kg \cdot m^{-3}$
σ_c = collision diameter, $\sigma_c = 0.5$ nm
ψ_0 = particle potential, mV

Literature Cited

Bacchin, P., P. Aimar, and V. Sanchez, "Model for Colloidal Fouling of Membranes," *AIChE J.*, **41**(2), 368 (1995).

Bowen, W. R., and F. Jenner, "Quantitative Models for Predicting the Rate of Ultrafiltration of Charged Colloidal Dispersions," in *Proc. of ICOM '93, Heidelberg, Germany* (1993).

Carnie, S. L., D. Y. C. Chan, and J. Stankovitch, "Computation of Forces between Spherical Colloidal Particles: Non Linear Poisson-Boltzmann Theory," *J. Colloid Interf. Sci.*, **165**, 116 (1994).

Cohen, R. D., and R. F. Probstein, "Colloidal Fouling of Reverse Osmosis Membranes," *J. Colloid Interf. Sci.*, **114**(1), 194 (1986).

Elimelech, M., "Particle Deposition on Ideal Collectors from Dilute Flowing Suspensions: Mathematical Formulation, Numerical Solution, and Simulations," *Sep. Technol.*, **4**, 186 (1994).

Glendinning, A. B., and W. B. Russel, "The Electrostatic Repulsion between Charged Spheres from Exact Solutions to the Linearized Poisson-Boltzmann Equation," *J. Colloid Interf. Sci.*, **93**(1), 95 (1982).

Green, G., and G. Belfort, "Fouling of Ultrafiltration Membranes: Lateral Migration and the Particle Trajectory Model," *Desalination*, **35**, 129 (1980).

Happel, J., "Viscous Flow in Multiparticle Systems, Slow Motion of Fluids Relative to Beds of Spherical Particles," *AIChE J.*, **4**(2), 197 (1958).

Hampton, J. H. D., S. B. Savage, and R. A. L. Drew, "Experimental Analysis and Modeling of Slip Casting," *J. Am. Chem. Soc.*, **71**(12), 1040 (1988).

Hull, M., and J. A. Kitchener, "Interaction of Spherical Colloidal Particles with Planar Surfaces," *Trans. Farad. Soc.*, **65**, 3093 (1969).

Jia, X., and R. A. Williams, "Particle Deposition at a Charged Solid-Liquid Interface," *Chem. Eng. Comm.*, **91**, 127 (1990).

Leonard, E. F., and C. S. Vassilieff, "The Deposition of Rejected Matter in Membrane Separation Processes," *Chem. Eng. Comm.*, **30**, 209 (1984).

Low Pressure Membrane Filtration for Particle Removal, Amer. Water Works Assoc., Chap. 4 (1992).

Lyklema, J., *Fundamentals of Interface and Colloid Science*, Chap. A9, Academic Press., Great Yarmouth UK (1991).

McDonogh, R. M., A. G. Fane, and C. J. D. Fell, "Charge Effects in the Cross-Flow Filtration of Colloids and Particulates," *J. Memb. Sci.*, **43**, 69 (1989).

McDonogh, R. M., K. Welsch, A. G. Fane, and C. J. D. Fell, "Incorporation of the Cake Pressure Profiles in the Calculation of the Effect of Particle Charge on the Permeability of Filter Cakes Obtained in the Filtration of Colloids and Particulates," *J. Memb. Sci.*, **72**, 197 (1992).

Michaels, A. S., "A New Separation Technique for the CPI," *Chem. Eng. Prog.*, **64**, 31 (1968).

O'Brien, R. W., and L. R. White, "Electrophoretic Mobility of a Spherical Colloidal Particle," *J. Chem. Soc. Faraday Trans. II*, **74**, 1607 (1978).

Press, W. H., B. P. Flannery, S. A. Teukolsky, and W. T. Vetterling, *Numerical Recipes*, Chap. 9, Cambridge Univ. Press, Cambridge, U.K. (1986).

Rodgers, V. G. J., and K. D. Miller, "Analysis of Steric Hindrance Reduction in Pulsed Protein Ultrafiltration," *J. Memb. Sci.*, **85,** 39 (1993).

Romero, C. A., and R. H. Davis, "Global Model of Cross-Flow Microfiltration Based on Hydrodynamic Particle Diffusion," *J. Memb. Sci.*, **39,** 157 (1988).

Ruckenstein, E., and D. C. Prieve, "Rate of Deposition of Brownian Particles Under the Action of London and Double Layer Forces," *J. Chem. Soc. Farad. Trans. II*, **69,** 1522 (1973).

Sader, J. E., S. L. Carnie and D. Y. C. Chan, "Accurate Analytic Formulas for the Double-Layer Interaction between Spheres," *J. Colloid Interf. Sci.*, **171,** 46 (1995).

Schmitz, P., B. Wandelt, D. Houi, and M. Hildenbrand, "Particle Aggregation at the Membrane Surface in Crossflow Microfiltration," *J. Memb. Sci.*, **84,** 171 (1993).

Sherman, N. E., and J. D. Sherwood, "Cross-Flow Filtration: Cakes with Variable Resistance and Capture Efficiency," *Chem. Eng. Sci.*, **48**(16), 2913 (1993).

Tiller, F. M. and J. R. Crump, "Solid-Liquid Separation: An Overview," *Chem. Eng. Prog.*, **73**(10), 65 (1977).

Tiller, F. M., and C. D. Tsai, "Theory of Filtration of Ceramics: I. Slip Casting," *J. Am. Ceram. Soc.*, **69,** 882 (1986).

Van de Ven, Th. G. M., "Colloidal Hydrodynamics," in *Colloid Science*, Academic Press, London, p. 69 (1989).

Verwey, E. J. W., and J. Th. G. Overbeek, *Theory of the Stability of Lyophobic Colloids: the Interaction of Sol Particles Having an Electric Double Layer*, Elsevier, New York (1948).

Wenten, I. G., "Mechanism and Control of Fouling in Crossflow Microfiltration," *Filtr. and Sep.*, **32,** 252 (1995).

Wiese, R., and T. W. Healy, "Effect of Particle Size on Colloidal Stability," *Trans. Farad. Soc.*, **66,** 490 (1970).

Zick, A. A., and G. M. Homsy, "Stokes Flow through Periodic Arrays of Spheres," *J. Fluid Mech.*, **115,** 13 (1982).

Zydney, A. L., and C. K. Colton, "A Concentration Polarization Model for the Filtrate Flux in Cross Flow Microfiltration of Particulate Suspension," *AIChE J.*, **47,** 1 (1986).

Manuscript received May 30, 1995, and revision received May 28, 1996.